

Hetero-epitaxy of Organic Nano-Fibers - The example of Ternaphthalene on Para-Hexaphenyl

Supplementary Information

Clemens Simbrunner,^{*,†} Günther Schwabegger,[†] Roland Resel,[‡] Theo
Dingemans,[¶] Francesco Quochi,[§] Michele Saba,[§] Andrea Mura,[§] Giovanni
Bongiovanni,[§] and Helmut Sitter[†]

*Institute of Semiconductor and Solid State Physics, Johannes Kepler University,
Altenbergerstrasse 69, A-4040 Linz, Austria, Institute of Solid State Physics, Graz University of
Technology, Petersgasse 16, A-8010 Graz, Austria, Faculty of Aerospace Engineering, Delft
University of Technology, The Netherlands, and Dipartimento di Fisica, Universita di Cagliari,
SLACS-INFN/CNR, I-09042 Monserrato (CA), Italy*

E-mail: clemens.simbrunner@jku.at

Force Field Simulations

In order to obtain the data for the presented force field calculations a self-written C program has been compiled. As starting point the force field parameters D_i [kcal/mol] and X_i [Å] for carbon ($D_{i,C}=0.105$ kcal/mol, $X_{i,C}=3.851$ Å) and hydrogen ($D_{i,H}=0.044$ kcal/mol, $X_{i,C}=2.886$ Å)

*To whom correspondence should be addressed

[†]Johannes Kepler University Linz

[‡]Graz University of Technology

[¶]Delft University of Technology

[§]Universita di Cagliari

have been taken from the universal force field (UFF).¹ In further consequence we have assumed a dominant van der Waals interaction which has been expressed by a Lennard-Jones 6-12 type potential:

$$E_{vdW} = D_{ij} \left\{ -2 \left(\frac{x_{ij}}{x} \right)^6 + \left(\frac{x_{ij}}{x} \right)^{12} \right\} \quad (1)$$

We have used a geometric mean combination rule for calculating the distance x_{ij} and energy D_{ij} parameters of two atomic species i, j following the recipe given by UFF.¹ The corresponding parameters are deduced by:

$$D_{ij} = \sqrt{D_i D_j}, x_{ij} = \sqrt{x_i x_j} \quad (2)$$

In a next step a $(11\bar{1})$ terminated para-hexaphenyl (p-6P) crystal stack has been generated based on the atomic positions and unit cell parameter of its equilibrium bulk structure.² A value of 20 Å has been chosen as cutoff distance for force field calculations. Based on the latter side condition a p-6P stack of $70 \times 120 \times 20$ Å³ has been generated, including $\approx 20,000$ hydrogen and carbon atoms. The height value of the upper most hydrogen atoms is taken as reference ($h=0$ Å).

In a further step binding energies $E_{vdW}(u,v,h)$ for carbon and hydrogen atoms are calculated where $u=\{0,0.01,0.02,\dots,99\}$; $v=\{0,0.01,0.02,\dots,0.99\}$; $h=\{-6 \text{ Å}, -5.8 \text{ Å}, \dots, 18 \text{ Å}\}$. Consequently a mesh of $100 \times 100 \times 121$ points is generated for each atom type. The corresponding real space coordinates x, y can be deduced by multiplication of (u,v) with the surface unit cell matrix of p-6P $(11\bar{1})$: $\{\{9.8218, 3.5932\}; \{0, -26.0921\}\}$ Å.

For a better visualization fig. 1 depicts the surfaces of equal binding energy for carbon (a) and hydrogen (b). The global energetic minima and consequently most favorable adsorption energies are calculated as $E_{min,C}=-98$ meV and $E_{min,H}=-49$ meV, respectively. As indicated by the magenta curves ($E_C=-86$ meV, $E_H=-43$ meV) the p-6P $(11\bar{1})$ surface is characterized by strong corrugations which are aligned parallel to the long molecular axes (LMA). As indicated by a side view along the smaller axis of the substrate surface unit cell, energetically preferred adsorption sites also follow

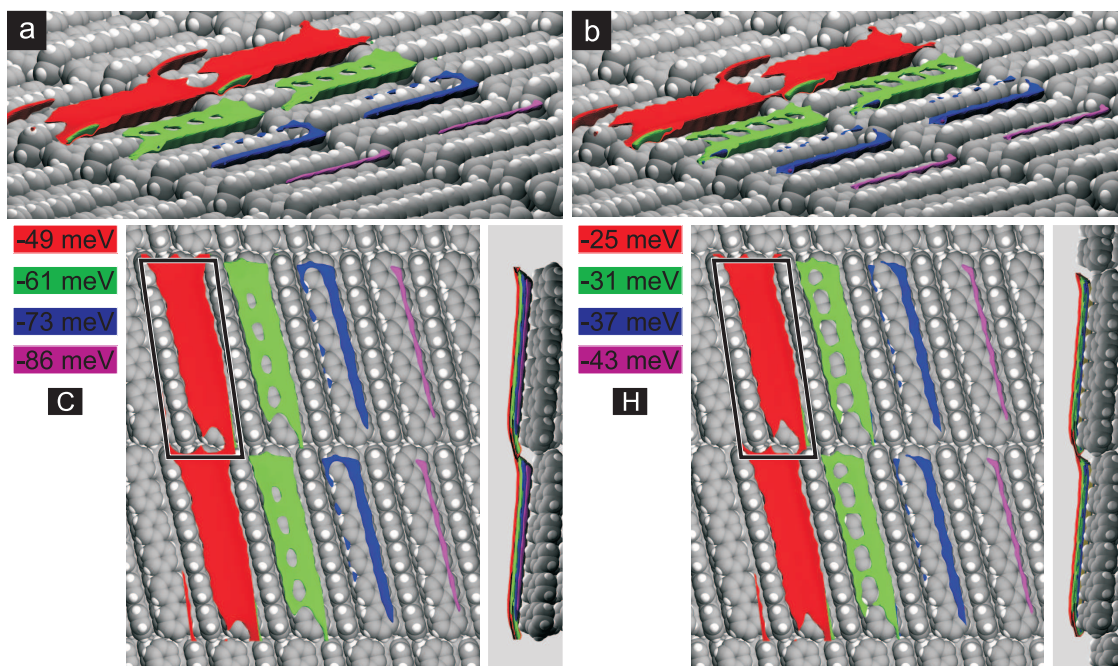


Figure 1: Surfaces of equal binding energy E_{vdW} for carbon (a) and hydrogen (b) atoms. Magenta surfaces indicate energetically preferable binding positions which are near to the energetic minima $E_{min,C}=-98$ meV, $E_{min,H}=-49$ meV.

the molecular alignment out of the substrate plane which can be explained by slight molecular tilt of p-6P relative to the substrate surface.

Based on the analysis presented in fig. 1 it can already be expected that chain like molecules which are shorter than p-6P will show a trend to align along the corrugation which is provided by the intersection of edge-on and flat-on p-6P molecules. Additionally it should be mentioned that $E_{vdW}(x,y,h)$ is highly asymmetric which can be explained by a tilt of the LMA and a slight non-parallel alignment of the phenyl rings (of the flat on p-6P molecules) relative to the substrate surface.

For the calculation of the molecular adsorption, the positions of carbon and hydrogen atoms have been deduced from a planar NNN molecule which has been extracted from its crystal structure.³ As a reference position the molecule has been rotated parallel to the substrate surface which is obtained by using a plane fit of the carbon atoms which span up the three naphthalene units. As indicated in the bottom part of fig. 2 the azimuthal reference position ($\varphi_z=0$) is chosen by a parallel alignment of the connection line of the outer most carbon atoms relative to the short axis of the

p-6P ($11\bar{1}$) substrate surface unit cell.

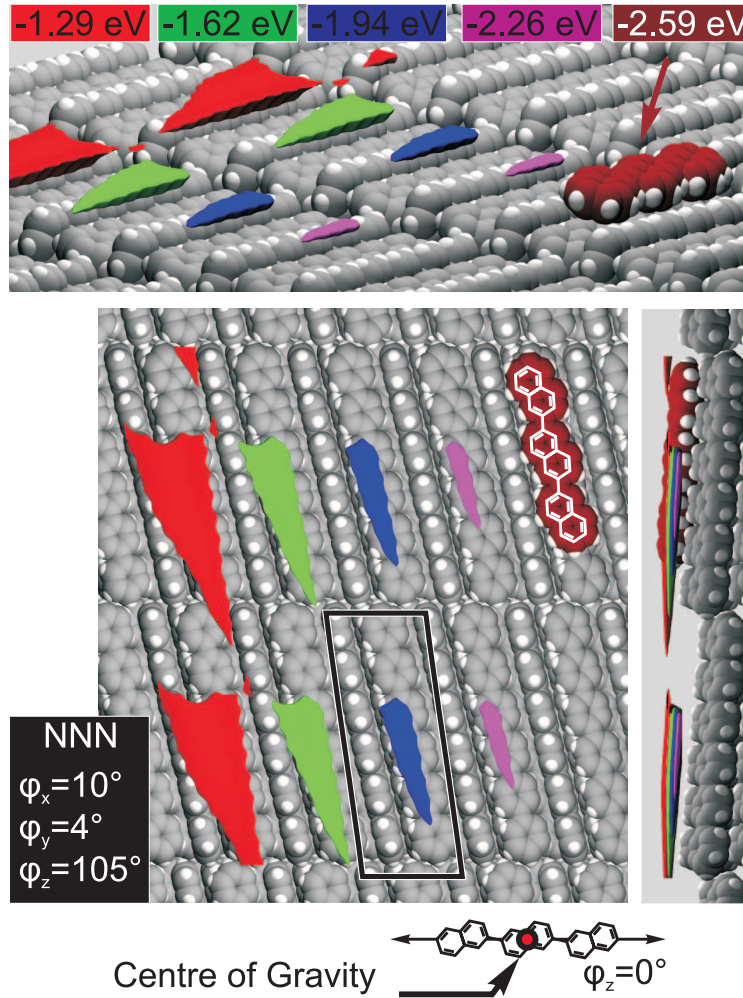


Figure 2: Surfaces of equal binding energy E_{vdW} for the energetically preferable NNN adsorption geometry ($\varphi_x=10^\circ$, $\varphi_y=4^\circ$, $\varphi_z=105^\circ$). Magenta surfaces indicate energetically preferable lateral positions of NNN's centre of gravity ($E=-2.26$ eV). The best adsorption position is indicated by an adsorbed NNN molecule ($E_{min,NNN}=-2.59$ eV). As indicated by an elongated shape, best adsorption energies can be obtained when moving the NNN molecule along the long molecular axis of p-6P in the surface corrugation. In the bottom part of the figure the azimuthal reference position ($\varphi_z=0^\circ$) for an NNN molecule is depicted, chosen parallel to the short axis of the p-6P ($11\bar{1}$) substrate surface unit cell.

The molecular centre of gravity has been chosen as reference point ($x_{mol}=0$, $y_{mol}=0$, $z_{mol}=0$) and consequently also represents the pivot for rotation. In order to calculate the molecular configuration for φ_x , φ_y , φ_z the positions of NNN's hydrogen and carbon atoms have been transformed by applying the rotational matrixes in the following order: φ_x , φ_y , φ_z . The resulting rotation matrix is

defined by:

$$\begin{pmatrix} \cos \varphi_y \cos \varphi_z & \cos \varphi_z \sin \varphi_x \sin \varphi_y - \cos \varphi_x \sin \varphi_z & \cos \varphi_x \cos \varphi_z \sin \varphi_y + \sin \varphi_x \sin \varphi_z \\ \cos \varphi_y \sin \varphi_z & \cos \varphi_x \cos \varphi_z + \sin \varphi_x \sin \varphi_y \sin \varphi_z & -\cos \varphi_z \sin \varphi_x + \cos \varphi_x \sin \varphi_y \sin \varphi_z \\ -\sin \varphi_y & \cos \varphi_y \sin \varphi_x & \cos \varphi_x \cos \varphi_y \end{pmatrix} \quad (3)$$

For the presented adsorption data of NNN, the binding energy for each combination of $\varphi_x = \{-180^\circ, -175^\circ, \dots, 180^\circ\}$; $\varphi_y = \{-20^\circ, -16^\circ, \dots, 20^\circ\}$; $\varphi_z = \{0^\circ, 5^\circ, \dots, 180^\circ\}$ has been optimized. This has been done by the following algorithm. After applying the corresponding rotation matrix, the molecule is positioned at $h=10 \text{ \AA}$. By applying the same resolution for u_{mol}, v_{mol} as chosen for the calculation of the reference binding energies of carbon (E_C) and hydrogen (E_H), the molecule is moved within the substrate surface unit cell (100×100 points). Again, real space coordinates for the translational movement are obtained by matrix multiplication of (u_{mol}, v_{mol}) with the substrate surface unit cell of p-6P ($11\bar{1}$). In a further step the x-y positions of all NNN atoms is projected back to the substrate surface unit cell of p-6P and corresponding binding energies are calculated by linear interpolation of the reference data (E_C, E_H). By summing up the binding energies of each NNN atom (30 carbon+20 hydrogen atoms), the molecular binding energy $E_{mol}(u, v, h=10 \text{ \AA})$ is obtained. In order to optimize the distance to the substrate surface, the molecule is continuously approached with steps of $\Delta h = -0.1 \text{ \AA}$ and the described procedure for calculating $E_{mol}(u, v, h)$ is repeated. The algorithm is stopped if all values $E_{mol}(u, v, h)$ have passed a minimum in adsorption energy versus adsorption height h . The obtained minimum value is further stored as best adsorption energy $E_{ad}(\varphi_x, \varphi_y, \varphi_z)$. The described procedure is further repeated for all molecular configurations, yielding $73 \times 11 \times 37 = 29711$ repetitions. The total calculation time on a single core of a Pentium IV (2.8 GHz) processor finally takes 14 hours.

For a better visualization fig. 2 depicts the obtained surfaces of equal binding energy for a NNN molecule which is characterized by $\varphi_x = 10^\circ$, $\varphi_y = 4^\circ$, $\varphi_z = 105^\circ$. The latter adsorption geometry represents the best solution obtained by the chosen steps of $\varphi_x, \varphi_y, \varphi_z$. The global energetic

minimum and consequently most favorable adsorption energy is calculated as $E_{NNN}=-2.59$ eV and is indicated by an adsorbed NNN molecule in fig. 2. The magenta surface ($E=-2.26$ eV) indicates a preferred adsorption geometry of NNN within the surface corrugation of p-6P ($11\bar{1}$). As NNN is characterized by a slightly shorter long molecular axis (LMA), the obtained surface of equal energy is characterized by an elongated shape. Moreover, as indicated by a side view along the smaller axis of the substrate surface unit cell, the molecular tilt of NNN nicely follows the p-6P template.

p-6P on p-6P ($11\bar{1}$)

In order to validate the chosen force field parameters and assumptions (dominant vdW forces), we have simulated the adsorption of a single p-6P molecule on a p-6P ($11\bar{1}$) template layer. As described above, the adsorption energies E_{ad} has been calculated for various molecular configurations determined by φ_x , φ_y and φ_z . Obtained results are indicated in fig. 3 in terms of colour coded 2D graphs presenting E_{ad} versus φ_x , φ_z (top) and φ_y , φ_z (bottom), respectively.

Fig. 3 (top) indicates the adsorption energy of p-6P on p-6P ($11\bar{1}$) depending on the herring bone stacking angle (φ_x) and azimuthal orientation (φ_z). The most favourable adsorption geometries are indicated by blue coloured regions. Consequently, the representation underlines a preferred azimuthal alignment of p-6P for $\varphi_z=105^\circ$. As sketched in fig. 4, which indicates a real space model of the adsorption geometries labeled by A-D, the latter geometry nicely correlates with a parallel alignment of the probed p-6P molecule relative to the molecular orientation within the organic template layer. Moreover, it should be mentioned that the obtained adsorption minimum is very well defined and sharp along φ_z whereas the adsorption energy only marginally changes for different herring bone angles φ_x . This impression is further underlined by the graphical representation of E_{ad} versus φ_x which is depicted beside. As indicated by an arrow (C), the best adsorption geometry ($E_{ad}=-3.14$ eV) is obtained for $\varphi_x=15^\circ$ which nicely reflects the molecular arrangement of flat on molecules within a p-6P ($11\bar{1}$) crystal stack.

The bottom part of fig. 3 depicts an analogous representation for E_{ad} versus LMA's tilt angle

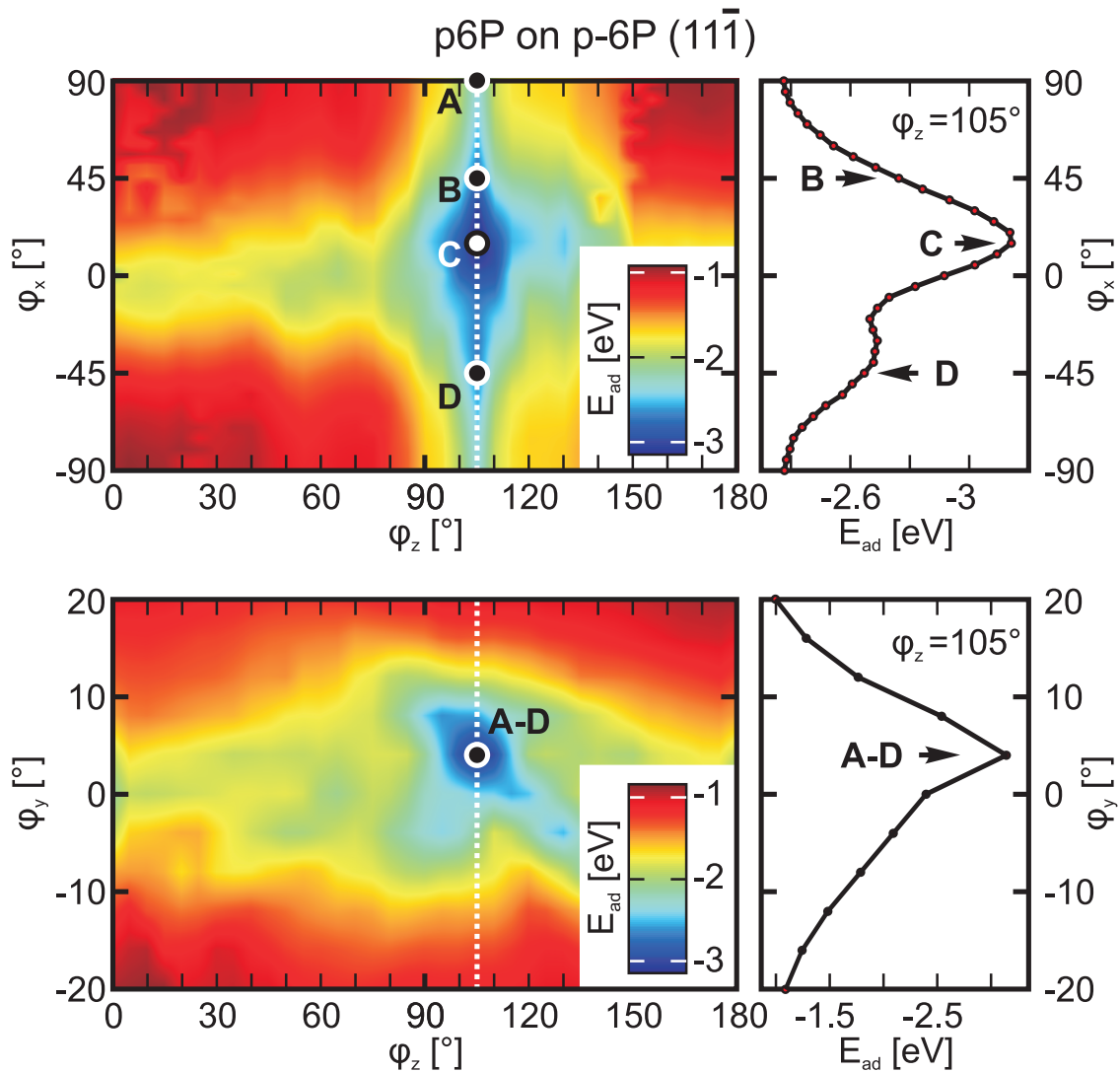


Figure 3: Top: Colour coded adsorption energy $E_{ad}(\phi_x, \phi_z)$ of a single p-6P molecule on a p-6P ($11\bar{1}$) template layer. For each datapoint the best adsorption configuration concerning the molecular tilt angle ϕ_y has been chosen. The colour coded representation indicates a clear and sharp minimum at $\phi_z=105^\circ$ which represents a parallel alignment of the probed p-6P molecule relative to the p-6P molecules within the template layer. Whereas E_{ad} is relatively sharp along ϕ_z , it is smeared out along ϕ_x indicating comparable adsorption energies for all herring bone angles. The latter impression is further underlined by the graph beside which presents the adsorption energy E_{ad} versus herring bone angle ϕ_x at the optimized azimuthal orientation ($\phi_z=105^\circ$). The best adsorption geometry is found at $\phi_x=15^\circ$ (C) which indicates a parallel stacking of the phenyl rings relative to the flat on molecules of the p-6P ($11\bar{1}$) substrate surface. Bottom: Analogous representation for E_{ad} versus the tilt angle ϕ_y of the long molecular axis relative to the substrate surface. In contrast to the $E_{ad}(\phi_x)$, the adsorption energy is characterized by a deep minimum at $\phi_y=4^\circ$ along both axes ϕ_y and ϕ_z , respectively. Again, the obtained value corresponds to the molecular tilt angle within a p-6P ($11\bar{1}$) stack.

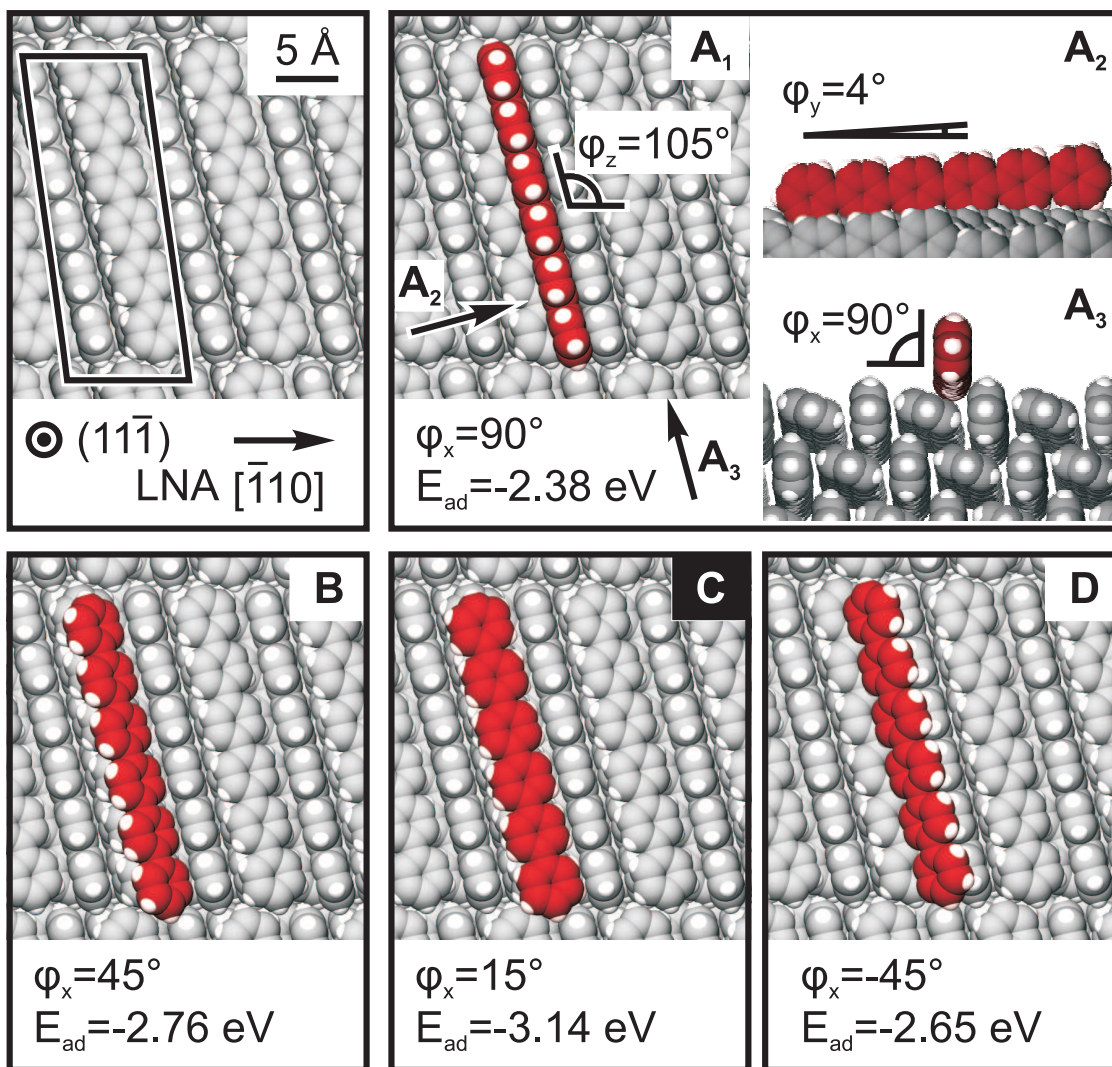


Figure 4: Real space model of the calculated molecular adsorption geometries A-D. The substrate surface unit cell of p-6P is also indicated in the top, left panel. Moreover, the geometrical alignment of φ_x , φ_y , φ_z is explained based on the edge-on molecular configuration A. Whereas φ_z correlates with the azimuthal alignment of the long molecular axis (LMA, A_1), φ_y (A_2)/ φ_x (A_3) are a finger print for the tilt of the LMA relative to the substrate surface/herring bone stacking angle.

(φ_y) and φ_z . In contrast to the previous discussion, the global adsorption minimum is well localized at $\varphi_y=4^\circ$, $\varphi_z=105^\circ$ along both axes. Again the obtained value nicely correlates with the molecular tilt relative to the substrate surface within a p-6P ($11\bar{1}$) crystal stack.

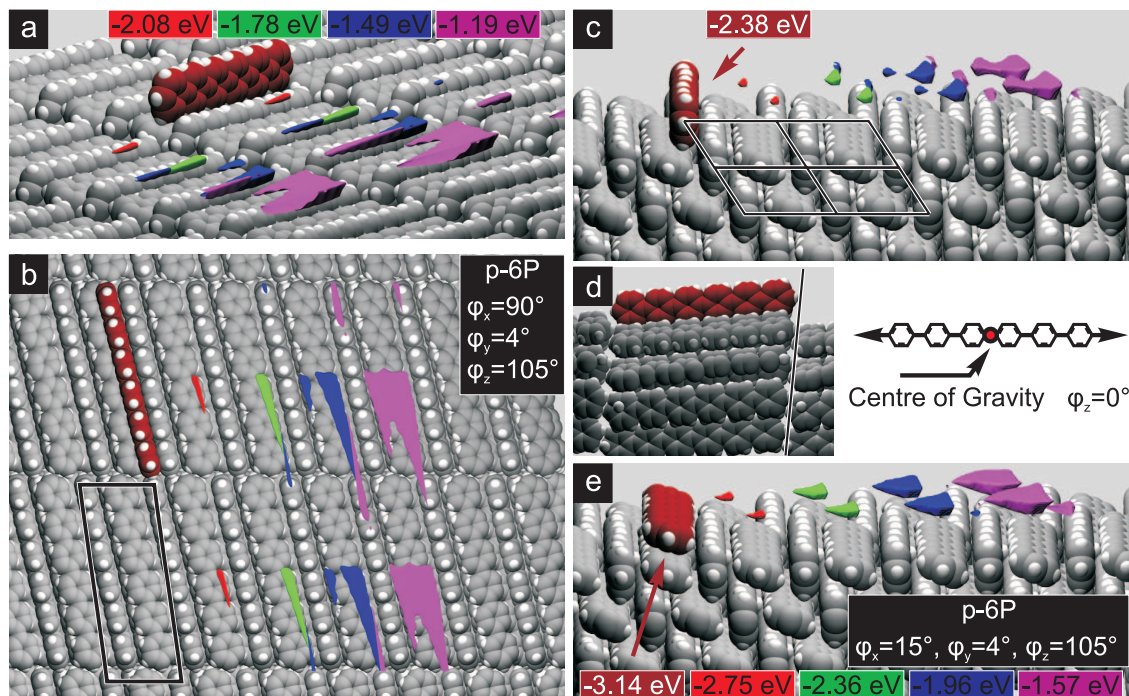


Figure 5: a)-d) Detailed analysis of the obtained p-6P edge-on adsorption geometry (compare fig. 3A, fig. 4A). a) A side view onto the p-6P ($11\bar{1}$) template stack. The red molecule indicates the optimized adsorption configuration ($E_{ad}=-2.38$ eV) for $\varphi_x=90^\circ$, $\varphi_y=4^\circ$ and $\varphi_z=105^\circ$. Coloured objects indicate surfaces of equal adsorption energy. The corresponding values for E_{ad} are indicated in the top part of the figure. b) A top view onto the crystal stack underlines a preferred adsorption of p-6P within the surface corrugation. c) A side view along the long molecular axis of p-6P underlines a perfect estimation of the p-6P adsorption distance based on the used force field parameters. d) The same holds true for the obtained molecular shift in stacking direction. The orientation of the p-6P (001) low energy plane is indicated by a black line. As indicated by the molecular structure, $\varphi_z=0$ correlates with a parallel alignment of the long molecular axis along the shorter surface unit cell vector of the p-6P template. e) Side view onto the best adsorption geometry obtained by calculations ($\varphi_x=15^\circ$, $\varphi_y=4^\circ$ and $\varphi_z=105^\circ$).

NNN on p-6P ($11\bar{1}$)

As discussed in the previous section for the adsorption of a single p-6P molecule on a ($11\bar{1}$) p-6P template layer, analogous calculations have been performed for a NNN molecule. For a better

comparison with the results obtained for p-6P, the obtained results are summarized in fig. 6 and fig. 7. A detailed discussion on the simulations of NNN can be found in the manuscript.

Simulations of a closed monolayer

Whereas, simulations performed for single p-6P and NNN molecules have revealed clear energetic minima for a parallel molecular orientations of p-6P as well as NNN relative to the p-6P molecules of the $(11\bar{1})$ template layer, the obtained results do not take into account molecule-molecule interactions which are responsible for the formation of the herring bone stacking. Consequently, the simulation program has been modified for the simulation of an infinite expanded first monolayer (ML) coverage. In particular the best adsorption energy has been calculated for $n=2$ rigid molecules (M_1, M_2) per surface unit cells which are positioned on a solid p-6P $(11\bar{1})$ substrate surface. In order to reduce the number of calculation steps, the azimuthal orientation $\varphi_{z,M1-M2}=104^\circ$ and molecular tilt angle relative to the substrate surface $\varphi_{y,M1-M2}=4^\circ$ have been kept constant at the optimized values obtained for single molecules.

Consequently, the herring bone tilt angles $\varphi_{x,M1}, \varphi_{x,M2}$, the lateral distance between both molecules $\Delta x=x_{M1}-x_{M2}, \Delta y=y_{M1}-y_{M2}$ and the distances of both molecules z_{M1}, z_{M2} relative to the p-6P substrate have been optimized. As variation steps for $\varphi_x, 5^\circ$ have been chosen. A closed ML is simulated by a translational shift of both molecules by the unit cell vectors of the p-6P $(11\bar{1})$ surface unit cell. For each tested configuration the adsorption energy per molecule is calculated as the sum of $E_{mol-sub}=\frac{1}{n}(E_{mol-sub,M1}+E_{mol-sub,M2})$ and $E_{mol-mol}=\frac{1}{n}(E_{mol-mol,M1}+E_{mol-mol,M2})$ where $n=2$.

In order to ensure the testing of a global minimum, the system has been optimized for 361 different starting conditions of $\varphi_{x,M1}, \varphi_{x,M2}$. Obtained results are shown in fig. 8 for a ML of p-6P and NNN, yielding four solutions for each system. The solutions A-D are sorted by the obtained binding energies and A represents the most preferable configuration. As indicated by the real space model of the simulated molecular species (red) on top of the p-6P substrate (grey) the energetically most favourable solutions is represented by the continuance of the herring bone stacking of the p-6P template. The obtained herring bone angles are indicated in the top right part

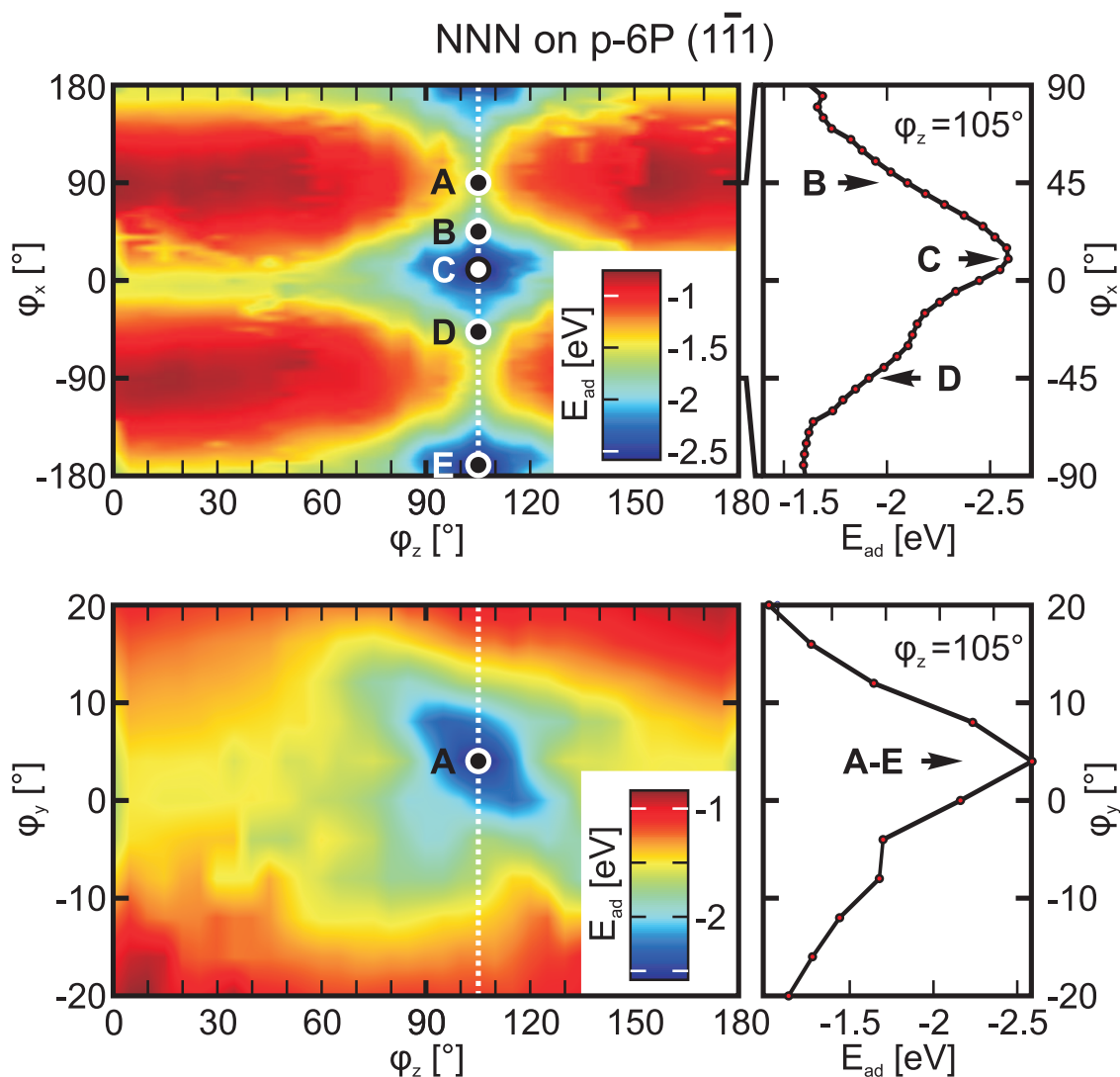


Figure 6: Top: Colour coded adsorption energy E_{ad} (ϕ_x , ϕ_z) of a single NNN molecule on a p-6P ($1\bar{1}\bar{1}$) template layer. For each datapoint the best molecular tilt angle ϕ_y has been chosen. The colour coded representation indicates a clear and sharp minimum at $\phi_z=105^\circ$ which represents a parallel alignment of the probed NNN molecule relative to the p-6P molecules within the template layer. Whereas E_{ad} is relatively sharp along ϕ_z , it is smeared out along ϕ_x indicated comparable adsorption energies for all herring bone angles. The latter impression is further underlined by the graph beside which presents the adsorption energy E_{ad} versus herring bone angle ϕ_x at the optimized azimuthal orientation ($\phi_z=105^\circ$). The best adsorption geometry is found at $\phi_x=10^\circ$ (C). Bottom: Analogous representation for E_{ad} versus the tilt angle ϕ_y of the long molecular axis relative to the substrate surface. In contrast to the E_{ad} versus herring bone angle, the adsorption energy is characterized by a deep minima at $\phi_y=4^\circ$. Again, the obtained value corresponds to the molecular tilt angle within a p-6P ($1\bar{1}\bar{1}$) stack. In contrast to p-6P, NNN does not provide a mirror symmetry plane, consequently ϕ_x has been probed for a 360° rotation to included also the upside down flipped NNN molecule (compare adsorption configurations C and E).

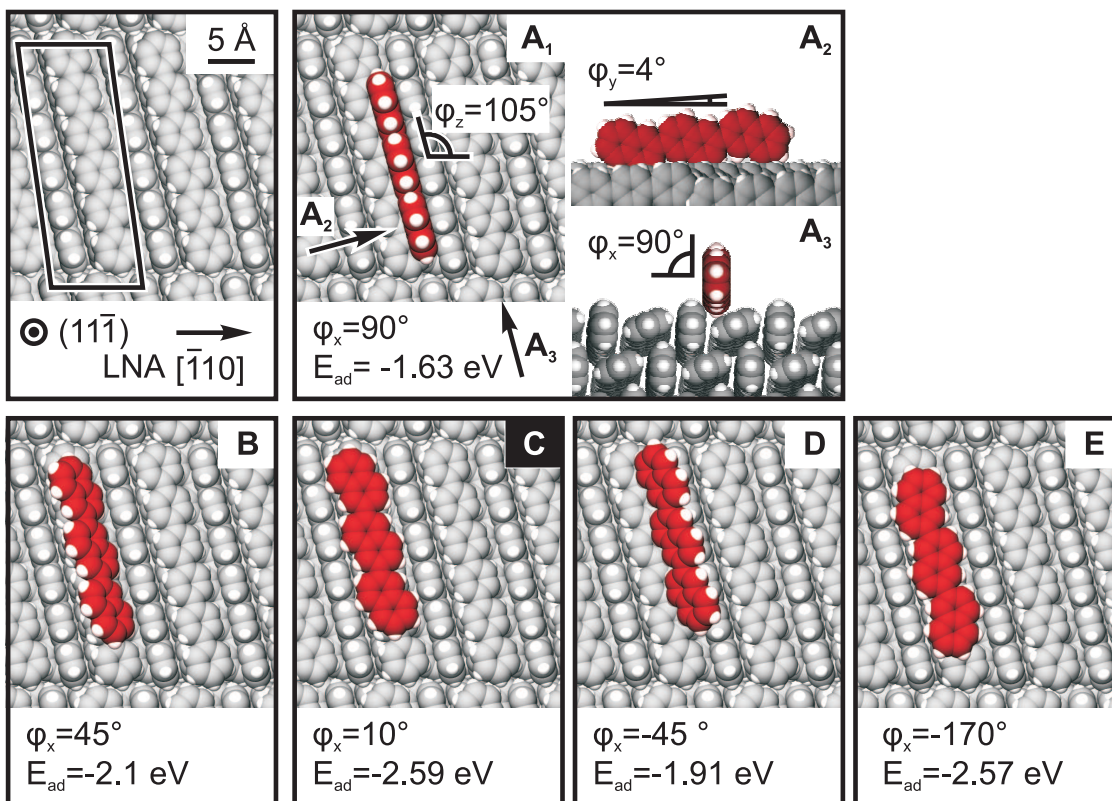


Figure 7: Real space model of the calculated NNN adsorption geometries A-E. The substrate surface unit cell of p-6P is also indicated in the top, left panel. Moreover, the geometrical alignment of ϕ_x , ϕ_y , ϕ_z is visualized based on the edge-on molecular configuration A. Whereas ϕ_z correlates with the azimuthal alignment of the long molecular axis (LMA, A_1), ϕ_y (A_2)/ ϕ_x (A_3) are a finger print for the tilt of the LMA relative to the substrate surface/herring bone stacking angle.

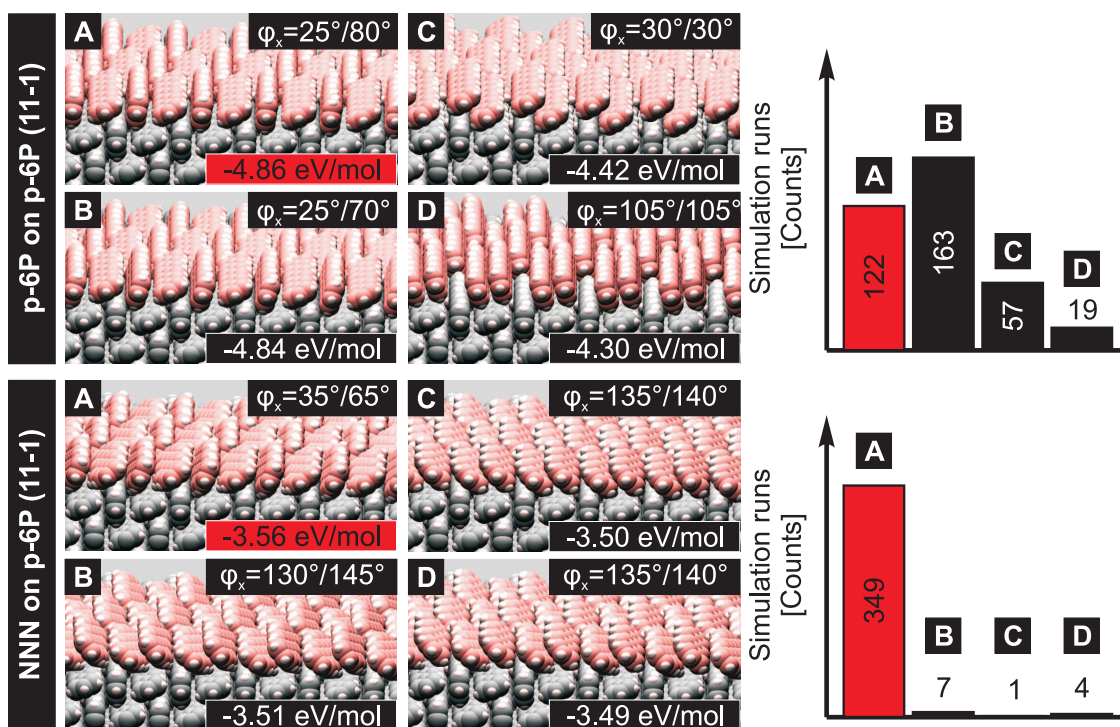


Figure 8: Obtained geometries for a closed monolayer (ML) of two p-6P (top)/NNN (bottom) molecules per surface unit cell on p-6P ($11\bar{1}$). The simulations reveal four different solutions (A-D) for 361 different starting conditions, where A represents the energetic most favourable adsorption geometry. The side panel of the figure depicts the frequency of occurrence for each solutions.

of each configuration, yielding $35^\circ/65^\circ$ for NNN on p-6P ($11\bar{1}$) which nicely correlates with the experimentally found (110) orientation of NNN ($31^\circ/82^\circ$).

Structural Investigations

In order to clarify the obtained crystal contact plane of NNN, X-ray diffraction (XRD) has been chosen and $\Theta/2\Theta$ scans were acquired:

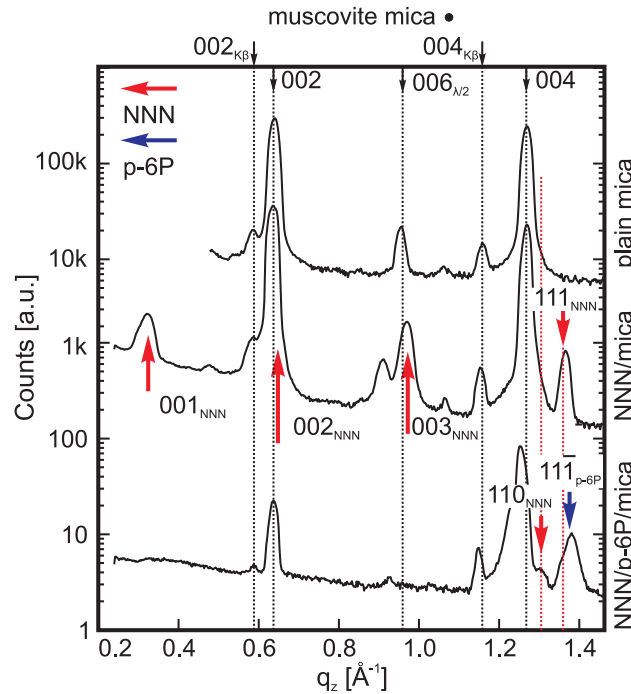


Figure 9: Specular diffraction scans of plain muscovite mica (top), NNN deposited on plain mica (centre) and NNN on p-6P template fibers (bottom). Black dotted lines indicate the peak positions of muscovite mica (001). Please note that the monochromator is transparent for λ , $\lambda/2$ and K_β . Whereas the specular scan of NNN/mica (red arrows) is dominated by a series of $(00n)_{NNN}$ diffraction peaks ($q_z=n \cdot 0.324 \text{ \AA}^{-1}$), no traces of standing molecular configurations can be found for NNN/p-6P. Additionally, (111) oriented NNN crystallites are found for NNN/mica (1.36 \AA^{-1}). In the case of NNN/p-6P a slightly shifted peak to higher q_z values (1.38 \AA^{-1}), characteristic for $(11\bar{1})$ of p-6P, arises (blue arrow). Additionally, a peak attributed to (110) of NNN at $q_z=1.31 \text{ \AA}^{-1}$ becomes visible.

Fig. 9 depicts a comparison of specular scans measured on plain muscovite mica (top), NNN deposited on plain mica (centre) and NNN on p-6P template fibers (bottom). Black dotted lines indicate the peak positions of muscovite mica (001). Please note that the monochromator is trans-

parent for λ , $\lambda/2$ and K_β . As indicated in fig. 9 (centre) by red arrows, located at $q_z = n \cdot 0.324 \text{ \AA}^{-1}$, the specular scan of NNN/mica is dominated by a series of $(00n)_{NNN}$ diffraction peaks. As discussed elsewhere⁴ those peaks are characteristic for island like morphologies consisting of almost upright standing NNN molecules. Additionally, (111) oriented NNN crystallites are found for ($q_z = 1.36 \text{ \AA}^{-1}$), which indicates a lying molecular configuration.

Contrary, in the case of NNN/p-6P a slightly shifted peak to higher q_z values (1.38 \AA^{-1}) arises (indicated by a blue arrow) which is characteristic for $(11\bar{1})$ oriented p-6P crystallites.⁵ Additionally, a peak attributed to (110) of NNN at $q_z = 1.31 \text{ \AA}^{-1}$ becomes visible. The latter contact plane is also characteristic for almost lying p-6P molecules.

X-Ray Diffraction Pole Figure Analysis

In order to discuss the diffraction pattern obtained by XRD-PF measurements, fig. 10a visualizes a real space model of the molecular packing within a $(11\bar{1})$ oriented p-6P crystallite. The fast growth direction $[1\bar{1}0]$, which is characterized by the zone axis of the p-6P (001) low energy plane and $(11\bar{1})$ contact plane, determines the long needle axis (LNA) of the generated nano-fibers.⁶ Contrary, the long molecular axis (LMA) can be approximated by the [302] crystallographic direction of p-6P.⁶ The oblique surface unit cell is sketched by a white polygon to underline the molecular tilt of $\approx 5^\circ$ out of the contact plane. For a better visualization, the lower panel of fig. 10a depicts a side view along the LNA direction.

Beside the molecular tilt out of the $(11\bar{1})$ crystal contact plane, it can also be recognized that p-6P molecules do not pack perfectly orthogonal to the LNA, but are slightly tilted by $\approx 15^\circ$.⁵ For further discussions, a graphical sketch of a p-6P crystal is indicated in the right panel of fig. 10a. The red box symbolizes a perfect cuboid oriented along the LNA to stress the generated oblique angles of the p-6P molecules within the stack, indicated by yellow shaded objects. The blue plane shows the orientation of the $(\bar{1}11)$ netplanes which are probed by XRD-PF measurements presented in the manuscript. At this point it should be mentioned that $(\bar{h}k\bar{l})$ and (hkl) netplanes are characterized by an equivalent interplanar distance due to the presence of a glide plane for both,

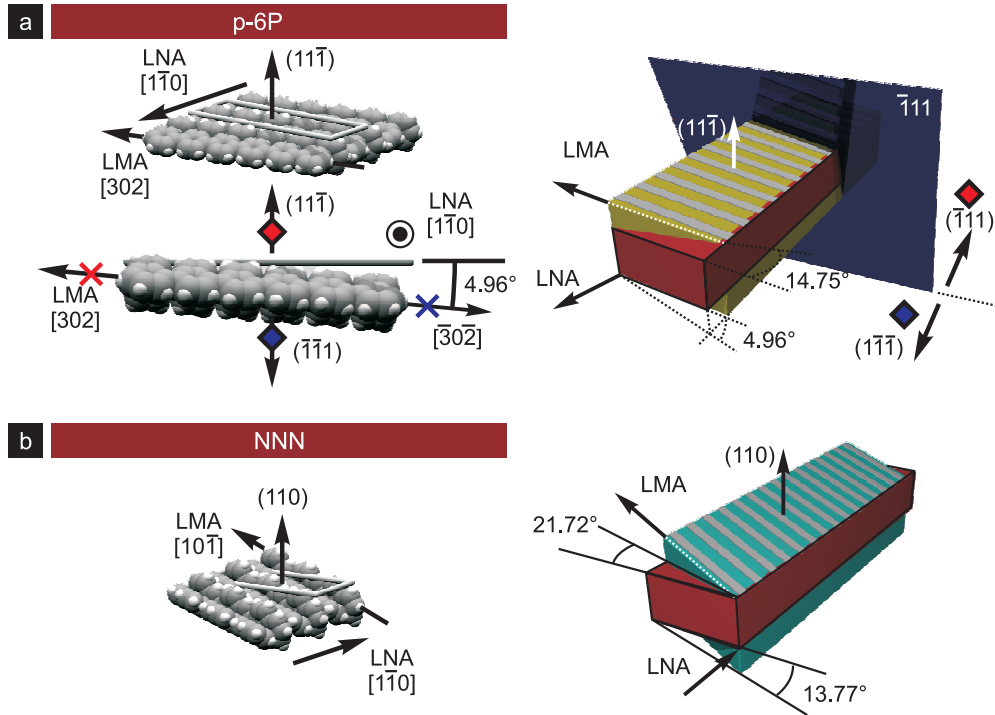


Figure 10: a) Graphical sketch of the molecular packing within a $(11\bar{1})$ oriented p-6P crystallite. The surface unit cell is sketched by a grey polygon. Whereas the long molecular axis (LMA) can be approximated by the $[302]$ direction, the long needle axis (LNA) is described by $[1\bar{1}0]$. As depicted by a side view along the LNA in the lower panel, molecules are tilted $\approx 5^\circ$ out of the contact plane. The right panel depicts a graphical sketch of the p-6P crystal characterized by a red box. As indicated by the yellow shaded object, additionally to a tilt out of the contact plane, the LMA is not perfectly orthogonal to the LNA but $\approx 15^\circ$ tilted. The blue plane indicates the alignment of $(\bar{1}11)$ netplanes probed by XRD pole figure measurements. Poles and crystallographic directions located in the upper (lower) hemisphere for a $(11\bar{1})$ orientation are marked by red (blue) symbols. b) Analogous representation for a NNN (110) oriented crystallite. The surface unit cell is sketched by a grey polygon. Whereas the long molecular axis (LMA) can be approximated by the $[10\bar{1}]$ direction, the long needle axis (LNA) is described by $[1\bar{1}0]$. NNN molecules are tilted $\approx 14^\circ$ out of the contact plane. The right panel depicts a graphical sketch of the NNN crystal characterized by a red box. As indicated by the cyan shaded object, additionally to a tilt out of the contact plane, the LMA is not perfectly orthogonal to the LNA but $\approx 22^\circ$ tilted.

p-6P² and NNN³ crystallites. Consequently, for both crystal types two poles in each, the upper and lower, hemisphere will arise except when (h0l) netplanes are probed. For a better visualization, crystallographic orientations [hkl] and poles (hkl) which are located in the upper hemisphere for a (11 $\bar{1}$) oriented p-6P crystal are indicated by red symbols whereas $[\bar{h}k\bar{l}]$ and $(\bar{h}k\bar{l})$ are marked by blue colour.

Analogous to previous discussion on p-6P, fig. 10b depicts the molecular packing of NNN within a (110) oriented crystal. The LMA can be approximated by the $[10\bar{1}]$ crystallographic direction whereas the LNA is characterized by $[1\bar{1}0]$. In the latter configuration NNN molecules are tilted by $\approx 14^\circ$ out of the contact plane. Molecules do not pack perfectly orthogonal to the LNA axis but are tilted by an angle of $\approx 22^\circ$ as indicated by the sketched stack in the right panel of fig. 10b. In order to distinguish the modelled NNN stack from p-6P crystallites, tilted NNN molecules are typified by cyan shaded objects.

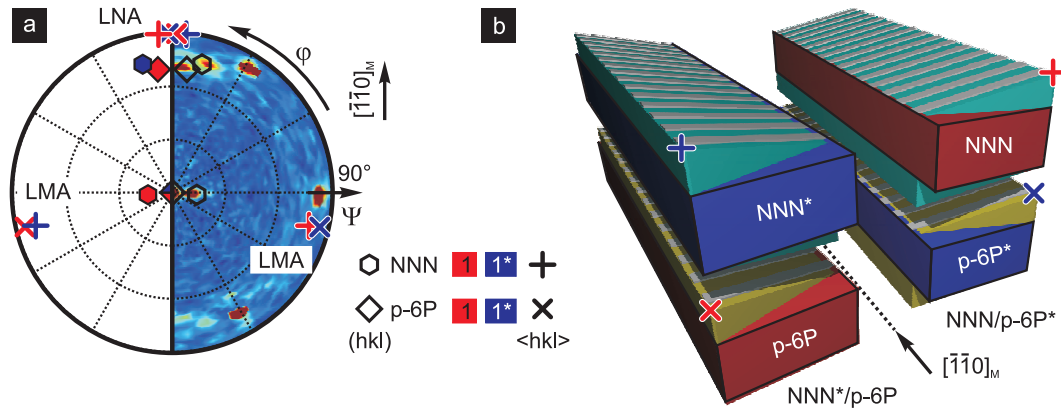


Figure 11: a) Precise fit for the dominant crystal fraction of p-6P/NNN of the XRD-PF acquired with a maximum sensitivity to $\{111\}_{NNN}$ netplanes. Hexagons (rectangles) represent diffraction peaks stemming from NNN (p-6P). The resulting long needle axes (LNA) and long molecular axes (LMA) orientations are indicated by red/blue crosses. b) Real space model of the deduced p-6P* ($\bar{1}\bar{1}1$)/NNN (110), p-6P (11 $\bar{1}$)/NNN* ($\bar{1}\bar{1}0$) crystal configurations. The dominant crystal fraction is characterized by two p-6P/NNN crystal pairs, mirror symmetric aligned relative to the $[1\bar{1}0]_M$ crystallographic direction of the muscovite mica substrate.

Fig. 11a depicts a precise fit of the XRD-PF which was acquired with a maximum sensitivity to $\{111\}_{NNN}$ netplanes ($q=1.36 \text{ \AA}^{-1}$). Only the dominant crystal fractions (1,1*) are taken into account. The acceptance angle of the XRD setup allows a simultaneous detection of $\{11\bar{1}\}_{p-6P}$

diffraction peaks. Diffraction peaks stemming from p-6P (NNN) are marked by rectangles (hexagons). Obtained LNA and LMA orientations are also indicated by crosses.

Based on the azimuthal orientation deduced from XRD-PF measurements, fig. 11b depicts a real space model of the p-6P* ($\bar{1}\bar{1}1$)/NNN (110), p-6P ($11\bar{1}$)/NNN* ($\bar{1}\bar{1}0$) crystal pairs. Nucleated hetero-structures are aligned mirror symmetric along the $[\bar{1}\bar{1}0]_M$ crystallographic direction of the muscovite mica substrate. This orientation coincides with the mirror symmetry plane of an α -terminated⁵ muscovite mica surface.

Fig. 12a depicts a simulated top view onto the p-6P* surface. Additionally, the corresponding crystallographic orientations are indicated in fig. 12a which span up the p-6P surface unit cell.

Based on the molecular configuration of the p-6P unit cell, the orientation of the phenyl rings and consequently herring bone angles can be approximated by the alignment of ($\bar{2}13$) for edge on and ($\bar{2}\bar{1}3$) for tilted p-6P molecules.⁶ As the LMA $[\bar{3}0\bar{2}]_{p-6P}$ is defined as the zone axis of both crystallographic planes, surface normals of the phenyl rings (blue squares) and LMA (blue cross) enclose an angle of 90° . The latter geometrical relationship is sketched in the stereographic projection of fig. 12a by two solid black arcs representing the equator and meridian of a sphere which north pole is oriented along the p-6P's LMA orientation. For a better visualization a 3D model for a tilted p-6P molecule is also indicated in the right panel of the figure. Calculated values for both the herring angles and LMA tilt relative to the substrate surface are listed in tab. 1 for a ($\bar{1}\bar{1}1$) p-6P crystal.

Table 1: Herring bone angles and tilt of the long molecular axis relative to the substrate surface.

Crystal	edge on [$^\circ$]	tilted [$^\circ$]	LMA [$^\circ$]
p-6P* ($\bar{1}\bar{1}1$)	90	21	4.8
NNN (110)	82	31	10.9
NNN Simulation	65	35	4
NNN ($\bar{1}\bar{1}\bar{1}$)	77	25	2.14

By applying analogous considerations for the orientation of the naphthalene rings within a NNN (110) crystal, the orientation of their surface normals can be determined (indicated by red hexagons in fig. 12a). Calculated values (82° , 31°), which are also listed in tab. 1, further underline a nice

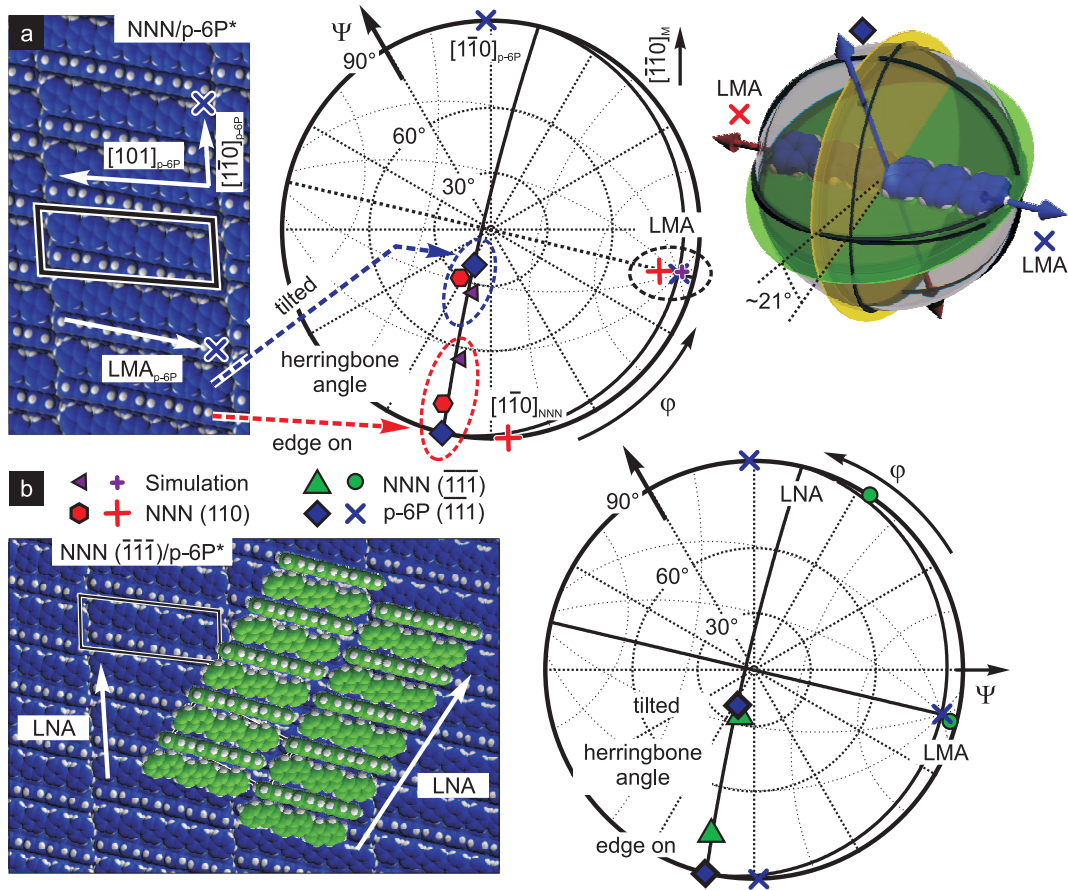


Figure 12: a) Sketch of the molecular alignment of a p-6P* substrate surface. The substrate surface unit cell and -vectors are also indicated. The stereographic projection beside visualizes the geometrical alignment of the LMAs, LNAs and herring bone angles for the modeled NNN/p-6P* stack. Herring bone angles are visualized by the surface normals spanned up by the phenyl- (p-6P*, blue square) and naphthalene (NNN, red hexagon) rings. For a better visualization a 3D sketch is indicated beside. A purple cross and triangles indicate the orientation of the LMA and herring bone angles obtained by force field simulations for a monolayer of NNN. b) Simulated top view onto a $(\bar{1}\bar{1}\bar{1})$ oriented NNN stack on a $(\bar{1}\bar{1}\bar{1})$ p-6P template. As indicated in the stereographic projection beside, the azimuthal orientation of the NNN-stack was chosen to achieve a maximum geometrical overlap concerning herring-bone angles and LMA orientation. In order to provide such a geometrical overlap, the stacking direction (LNA) of NNN has to be tilted by $\approx 37^\circ$ relative to the LNA of the p-6P template.

correlation with the herring bone stacking sequence of the p-6P template stack (90° , 21°). The discrepancy can be understood by the different herring bone angles determined by the crystal structures of p-6P ($\approx 66^\circ$)⁶ and NNN ($\approx 53^\circ$).

For comparison, force field simulations have been performed for a closed monolayer of NNN molecules on top of a p-6P template stack. The obtained herring bone angles are indicated in fig. 12a by purple triangles and are listed in tab. 1.

Fig. 12b indicates a simulated top view onto a NNN ($\overline{111}$) crystal on a p-6P ($\overline{111}$) template layer. The azimuthal and orientational configuration of the NNN stack has been chosen to achieve a maximum geometrical overlap concerning the LMA orientation and herring bone stacking. The situation is visualized by a stereographic projection depicted beside. Blue rectangles indicate the orientation of the p-6P phenyl units, whereas blue crosses characterize the LNA and LMA orientation of p-6P. Contrary, green triangles represent the orientation of the naphthalene units of NNN and green filled circles the resulting LMA/LNA orientation.

Based on the graphical sketch it can be concluded that a geometrical overlap of NNN and p-6P can only be obtained for a ($\overline{111}$) oriented NNN crystal if the molecular stacking direction (LNA) is tilted by $\approx 37^\circ$ relative to the LNA of p-6P. As indicated by the simulated top view onto the p-6P/NNN stack in fig. 12b, the latter configuration implies a molecular alignment of NNN across step edges (compare side view depicted in fig. 1a-b) of the p-6P template surface. Contrary, the experimentally observed (110) orientation of NNN allows a nearly perfect adoption of the herring bone stacking angles, LMA orientation and, importantly, stacking direction. The latter observations explains most likely an energetically preferred formation of a (110) contact plane in contrast to the observed (111) orientation when deposited on plain muscovite mica.⁴

References

- (1) Rappi, A. K.; Casewit, C. J.; Colwell, K. S.; Goddard III, W. A.; Skid, W. M. *J. Am. Chem. Soc.* **1992**, *114*, 10024–10039.

- (2) Baker, K. N.; Fratini, A. V.; Resch, T.; Knachel, H. C.; Adams, W. W.; Socci, E. P.; Farmer, B. L. *Polymer* **1993**, *34*, 1571.
- (3) Pichler, A.; Resel, R.; Neuhold, A.; Zojer, E.; Dingemans, T.; Schwabegger, G.; Simbrunner, C.; Salzmann, I.; Moret, M. *Crystalline Materials (Zeitschrift für Kristallographie)* submitted.
- (4) Simbrunner, C.; Schwabegger, G.; Resel, R.; Dingemans, T.; Sitter, H. *Cryst. Growth Des.* **2014**, *14*, 442.
- (5) Resel, R.; Haber, T.; Lengyel, O.; Sitter, H.; Balzer, F.; Rubahn, H.-G. *Surf. Interface Anal.* **2009**, *41*, 764.
- (6) Simbrunner, C. *Semicond. Sci. Technol.* **2013**, *28*, 053001.